Applied Surface Science 615 (2023) 156382

Contents lists available at ScienceDirect

Applied Surface Science

journal homepage: www.elsevier.com/locate/apsusc

Full Length Article

Boron-doped diamond growth on carbon fibre: Enhancing the electrical conductivity

J. Millán-Barba [a,*], H. Bakkali [b], F. Lloret [c], M. Gutiérrez [a], R. Guzmán de Villoria [d], M. Domínguez [b], K. Haenen [e,f], D. Araujo [a]

[a] Dep. Materials Science and Metallurgical Engineering and Inorganic Chemistry, University of Cadiz, Spain
[b] Dep. Condensed Matter Physics and Institute of Electron Microscopy and Materials, University of Cadiz, Spain
[c] Department of Applied Physics, University of Cádiz, Spain
[d] FIDAMC, Foundation for Research, Development and Application of Composite Materials, Spain
[e] Institute for Materials Research (IMO), Hasselt University, Belgium
[f] IMOMEC, IMEC vzw, Diepenbeek, Belgium

ARTICLE INFO

Keywords:
Carbon fibres
Diamond coating
Boron doped
Electrical properties
Conductive atomic force microscopy
Scanning microwave impedance microscopy

ABSTRACT

Carbon fibre reinforced polymers (CRFP) are extensively used in many industrial applications thanks to its mechanical properties and its low weight. Nevertheless, the orthotropic character of CRFP highly reduces its applications. The transversal electrical conductivity in CRFP is two orders poorer than in the longitudinal direction. To improve their electrical properties, this work proposes the use of polycrystalline boron doped diamond (BDD) as coating of the carbon fibres (CF). BDD coating is deposited on CF surface using microwave plasma enhanced chemical vapor deposition (MPCVD) system. The BDD coating forms a rigid conductive coating around the CF as a core–shell structure. Here, an electrical characterization of both, 12,000 filaments (a tow) and a single coated filament, are carried out in the longitudinal and cross-section directions. Macro, micro and local analysis using the Kelvin method, Conductive Atomic Force Microscopy (C-AFM), and Scanning Microwave Impedance Microscopy (sMIM), were carried out to evidence the improvement of the electrical properties. Macro measurement reveals that the BDD coating decreases to half the resistivity of the CF. The BDD coating raises the local electrical conductivity of the CF by an order of magnitude with respect to the uncoated ones. sMIM maps identified BDD locations in ring-like configurations.

1. Introduction

Carbon fibre reinforced polymers (CFRP) is widely used in all areas where weight reduction offers a potential improvement in the economical and/or ecological performances. The high specific strength, stiffness, Young's modulus (200–600 GPa) and extraordinary dimensional stability make of the carbon fibres (CF) a promising high-performance engineering material for high-specification applications. The use of CF in areas as aerospace [1], transport [2] or sport [3] has become revolutionary and its implementation in new industries is promising [4].

Nowadays, the main efforts in CFRP research are focused in enhancing their properties and eliminating their weaknesses. Different approaches have been reported mainly based on a modification of the polymer matrix [5], coating the CF [6], or surface treatments [7]. Therefore, aspects as fibre surface modifications using multi-scale techniques are one of the main methodologies used. Increases of between 13 and 175% in interlaminar shear strength have been obtained by making stronger bonds fibre-polymeric matrix interface by coating the fibres with carbon nanotubes (CNTs) [8]. Coatings such as CNTs, boron nitride nanoparticles, copper or silver, have been shown to significantly improve the thermal and electrical conductivities through the thickness of the CFRP stack [9,10]. Zheng et al. [11] reported a 217% increase in in-plane thermal conductivity by hexagonal BN/Cu coating. Yamamoto et al. [12] obtained 6–8 orders of magnitude higher electrical conductivity by adding multi-walled CNTs to the CF surface. Nevertheless, CNTs growth damages the CF surface by reducing strength, strain-to-failure and the uneven coating distribution cannot be

* Corresponding author at: Universidad de Cádiz, Dpto. Ciencias de los materiales, CASEM, Despacho 23, Pala A, 1ª planta, Avda. República Saharaui, s/n, CP:11510, Puerto Real (Cádiz), Spain.
E-mail address: josue.millan@gm.uca.es (J. Millán-Barba).

https://doi.org/10.1016/j.apsusc.2023.156382
Received 25 October 2022; Received in revised form 16 December 2022; Accepted 6 January 2023
Available online 8 January 2023

avoided [13].

Coating modifications to the surface of CF become an active area of research with the aim of improving CF properties without compromising other characteristics. For this purpose, here, CF are coated by heavily boron-doped diamond (BDD) to improve the electrical conductivity of the CFRP composite. The boron incorporation in substitutional sites of the diamond lattice allows a p-type doping of the material and thus increase its electrical properties [14–16]. This increasing can be observed by electrical characterization techniques like, Kelvin probe or AFM, among other.

In fact, the excellent biocompatibility, mechanical hardness (∽100GPa), optical transparency, high bandgap (5.47 eV), thermal conductivity (2x10^3 W•m^{-1}•K^{-1}), chemical corrosion resistance and electrical insulator (10^{16} Ω•cm) [17,18] make diamond a useful material for a wide range of applications in the electronic, optical, mechanical, and biological fields. In addition, impurities can be incorporated into the diamond lattice to achieve better properties. Diamond is a good candidate as a coating to cover the CF [8]. In this line, the hybrid structures of CF and diamond are a very promising material for diverse applications such as micro-electrodes for bioelectronics, sensors, neuroscience, or electrochemistry. This is due to the combination of the low capacitive current, large potential window and low contaminant absorption of BDD, combined with the mechanical strength, chemical resistance and conductivity of CF [19,20].

Diamond deposition on different substrates (Si, SiC or WC, [21–24]) has become easier and more accessible [25], which makes possible the development of new diamond-based materials. Furthermore, the electrical behaviour of BDD coatings can be controlled during the growth process. J. Barjon et al. [26] reported comparative BDD resistivities as a function of boron incorporation in the diamond coating. They found an increase in electrical conductivity from 10^0 to 10^2 (Ω^{-1}•mm^{-1}) for the higher doping levels ([B] > 10^{20}cm^{-3}). Under these conditions, diamond become an electrically conductive material (metallic behaviour). Concerning diamond growth on different fibres, BDD growth on SiO_2-fibres have been reported by V. Petrák et al. [27] or Z. Vlčková Živcová et al. [28]. The use of such substrates makes possible to remove (chemical etching) the substrate to obtain diamond tubes or to fabricate multi "core–shell" like cylindrical structures. In addition, such step-by-step fabrication of BDD templates using spin coating of SiO_2 fibres on heteroepitaxial BDD through multi-steps growth provides a useful method to obtain high quality diamond (sp^3/sp^2 ratio). V. Petrák et al. characterises the electromechanical properties for applications as electrodes or supercapacitors. Where the voltammetric capacitance reaches ca. 7 mF/cm^2 with excellent stability, remaining at 85% of the initial value after 3000 cycles. On other hand, Z. Vlčková Živcová et al. studied the cyclic voltammetry and galvanostatic charge/discharge cycling of porous BDD electrodes in different electrolyte solutions. Obtaining the best capacitance of ca. 2mF/cm^2 in 0.5 M H_2SO_4 electrolyte solution.

To estimate the doping level in diamond, usually secondary ion mass spectroscopy (SIMS) [29,30] or cathodoluminescence [31,32] are used. However, these are very heavy experiments and recently, V. Mortet et al. propose a simpler way to obtain the boron doping level in diamond: Raman spectroscopy, which is a fast and appropriate contactless characterization method. For the case of diamond, the 1332 cm^{-1} Raman peak is widely known to correspond to sp^3 carbon bonds. It is usually used to evidence the diamond proportion in diamond like carbon materials [33]. The presence of boron modifies proportionally the position of this peak by a quantum interference between the phonon and a continuum of electronic state in a degenerate semiconductor (Fano effect) [34]. In addition, BDD Raman spectra show two characteristic broad bands located at ca. 500 cm^{-1} and 1200 cm^{-1}, caused by the vibration of the boron atoms. By analysing the double Fano effect of the diamond zone center line and the phonon density of states of the boron bands, the BDD Raman spectra can be related to the boron doping concentration [35]. This method is easier compared to SIMS and cathodoluminescence but less sensitive as it detects boron doping above 5 × 10^{19}cm^{-3}.

On the other hand, the electrical conductivity of CF is related to their microstructure and mechanical properties. CF produced from polyacrylonitrile (PAN) can be classified in the following categories according to their tensile modulus: standard grade 230–240 GPa, intermediate modulus 280–300 GPa (and high strength, HSCFS), high modulus 350–480 GPa (HMCFs) and ultrahigh modulus 500–600 GPa (UHMCFs). Table 1 lists the electrical conductivity of the CF in their longitudinal direction and the mechanical properties of different CF [36,37]. Consequently, comparing the electrical conductivities of CF in its longitudinal, they are at the limit between an electrically conductive material and a semiconductor (semiconductor range σ = 10^2-10^3 Ω^{-1}•mm^{-1}) [38].

In addition, the anisotropic nature of the properties of the CF composite material should be noted. It has lower electrical conductivity in the transverse direction than in the longitudinal direction of the fibres. The conductive BDD deposited on the CF is expected to improve the longitudinal electrical conductivity of the carbon fibre. Moreover, due to the percolation effect generated by the polycrystalline BDD coating between the fibres within the composite, the transverse electrical conductivity is also expected to improve.

This study focuses on the electrical characteristics of CF coated with BDD. Electrical conductivity has been studied by Kelvin probe method and conductive atomic force microscopy (C-AFM) using specifically designed setups. The cross-section conductivity on the fibres has been evaluated by scanning Microwave Impedance Microscopy (sMIM) to highlight the effect of the BDD coating.

2. Material and methods

2.1. Diamond growth

Tows of 12,000 commercial CF polyacrylonitrile (PAN) filaments ("HexTow AS7" from Hexcel Corporation) with a length of 5 cm and a nominal fibre diameter of 6.9 μm were used as substrate. This type of CF is commonly used in CFRP materials for aircraft manufacturing. The CF were pre-treated before diamond growth by immersion in an ultrasonic bath with a solution of 6–7 nm nanoparticles size diamond in deionized (DI) water [39,40]. Seven CF samples were diamond-coated on an ASTeX 6500 series microwave plasma enhanced chemical vapor deposition (MPCVD) reactor [41] using a gas mixture of methane, hydrogen, and trimethylborane (TMB). Table 2 summarize the growth conditions. The growth process has already been reported elsewhere [42].

The G7 sample lost the bond between the fibres due to handling. Therefore, G7 was used only for single fibres electrical measurements by C-AFM.

The surface of the grown samples was studied by SEM using a TESCAN Solaris Dual BEAM SEM-FIB microscope. In addition, the average area of the diamond coating (A_D) was estimated studying the coating in different areas of the tow by SEM.

To evidence the diamond phase, Raman spectra were recorded at room temperature in the back-scattering configuration using a Renishaw Raman spectrometer (System 1000) equipment. A blue laser illumination with 488 nm of excitation wavelength was used. The spectrometer was calibrated using the silicon F1g peak at 520.2 cm^{-1}.

Table 1
Carbon fibres electrical conductivity as function of tensile modulus.

Tensile Modulus (GPa)	Electrical conductivity (Ω^{-1}•mm^{-1})
230–240	58–65
280–300	70–75
350–480	100–110
500–600	110–140

Table 2
Growth conditions used during the MPCVD deposition of the nanocrystalline diamond (NCD) layers.

#	Power (kW)	Vacuum (Torr)	H_2 (sccm)	CH_4 (sccm)	TMB* (sccm)	Time (min)
G1	3.0	35	495	5	–	120
G2	3.0	40	395	5	100	600
G3	3.5	35	455	5	40	600
G4	3.5	40	455	5	40	600
G5	4.0	45	455	5	40	390
G6	3.5	45	455	5	40	720
G7	4.0	35	455	5	40	600

*Trimethylborane **(TMB)**.

2.2. Electrical measurements method

Kelvin probe method was carried out on a fibre tow placed horizontally on an insulating glass. Electrical contact points at the ends of the tow were created with conductive silver paint. A Matelect ISM5 induced signal monitor was used as power supply and for current measurements. An UNI-T UT89X digital multimeter was used to measure voltages [38]. Electrical measurements were carried out along uncoated and coated carbon filaments for comparison purposes.

C-AFM studies were carried out on single fibres fixed on a mica disc by a thin natural wax layer. Silver paste was used to connect one extreme of the fibre to the AFM metal holder disc. This silver contact allows current to flow in longitudinal direction of the filament. Fig. 1a shows the sample set up for C-AFM measurements. Topography and current maps were recorded in the forward scan direction, i.e. from left to right. The conductive working mode of BDD-CF surface was performed at a sample bias of + 500 mV using Park NX10 and NX20 AFM system. Conductive diamond coated tips CDT-NCHR (k = 80 N/m, f = 400 kHz) with a radius of curvature of the tip in the range of 100–200 nm were used. Measurements were performed using the system Quickstep, which keeps the tip force constant (600 nN), since the tip is held in place at each pixel for 4 ms. To perform these measurements, the tip was located at the same distance from the silver paste electrode in both uncoated and coated filaments [43].

Cross-sectional views of the BDD-CF stack were carried out by Scanning Microwave Impedance Microscopy (sMIM) to evidence the effect of the BDD coating on the composite's conductivity. For such a setup, the filaments were placed upright within an epoxy resin matrix (Fig. 1b). The epoxy resin supports the filaments and completely covers them. Through a sanding and polishing process, the resin was removed from the top. In this way, the cross-sectional surface of the filaments is shown upwards and with a smooth surface. The sample is glued to the metal disc by conducting silver paint. Therefore, the capacitance and conductance superficial variations between the CF core and BDD coating are simultaneously mapped by sMIM.

The sMIM tip is an antenna radiating at microwave frequencies (around 3 GHz) and scans the surface of the sample. The microwaves reflected from the surface are collected by a sensor that generates a signal of voltage intensity variations. Two dc-signals are obtained by demodulating the complex reflected signal. The real part corresponds to the resistive (sMIM-R) component, while the imaginary part corresponds to the capacitive (sMIM-C) component of the tip-sample admittance $Y = Z^{-1}$ [44]. Voltage variations are represented in a colour scale map. These measurements allow to qualitatively estimate the difference in surface electrical conductivity between the materials present on the surface of the sample [45].

- Data post-processing

The data collected were processed using the Gwyddion (version 2.55), ImageJ (version 1.53c) and Origin© 2018 software. Through the Gwyddion software, the measured AFM topographic and electrical maps were treated by applying the following tools to correct the data: Surface topography/current map measurements on uncoated and BDD-CF were processed by aligning rows and shifting the minimum data value to zero. The background line pattern in sMIM resistive signal maps was removed by applying masks and 2D FTT filter.

3. Results and discussion

BDD depositions were first studied by scanning electron microscopy (SEM). Fig. 2 shows SEM micrographs of the CF samples coated with BDD. Fig. 2a shows a low magnification micrograph of the inner part of the G4 sample. Fig. 2b enlarges this region and evidences the growth of BDD in the centre of the tow. Micrographs like those in Fig. 2a and 2b were used to estimate the diamond coating area (A_D) in all coated samples (Fig. 2c). Cross sectional SEM micrographs were carried out at different tows locations. Diamond covered fibre density and thickness have been estimated using ImageJ software on the SEM micrographs. From such procedure, diamond areas and thicknesses are compared (see Table 3).

Fig. 2d shows CF of sample G4 completely covered by nanocrystalline BDD. Nevertheless, the BDD coating is not uniform throughout the length of the fibre, varying in thickness. G1, G2, G5 and G7 samples exhibit the same BDD coating as G4. In contrast, G3 and G6 samples showed large areas covered by carbon nanowalls instead of BDD (See Fig. 2e). Carbon nanowalls has been reported to be an interlayer formed on the CF prior to diamond growth by MPCVD [42].

The diamond phase of the coating has been confirmed by Raman spectroscopy, as shown in Fig. 3. Raman spectra were taken at five different locations of each sample. A representative spectrum of each sample is shown in Fig. 3. As reference uncoated carbon fibre was measured. It exhibits the characteristics peaks at 1350 cm^{-1} and 1580

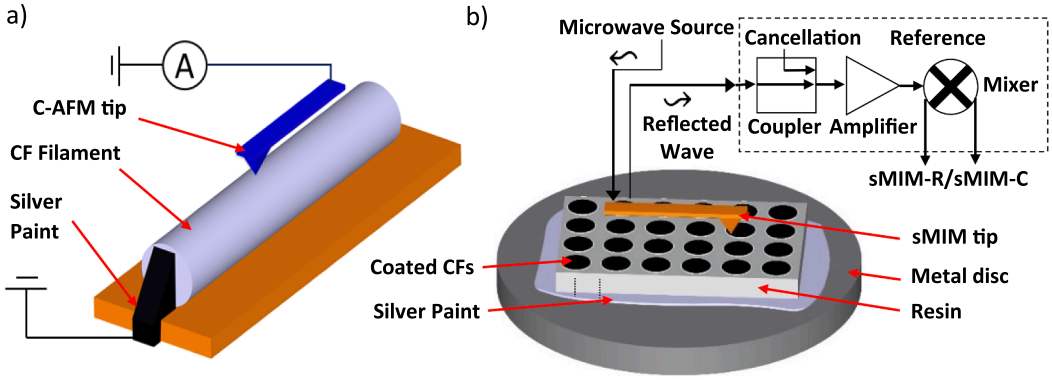

Fig. 1. a) Diagram of C-AFM experimet steup. A single filament liying in a insulate cristal with a metal contact in one extreme. b) Coated CF sample preapration in cross-section view for sMIM measurements.

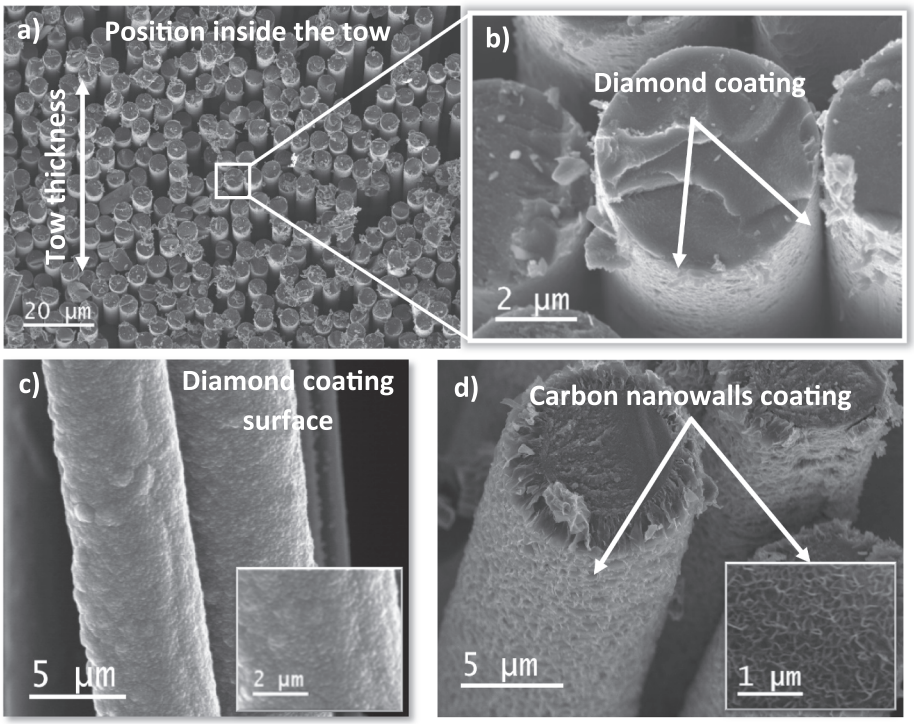

Fig. 2. a) SEM micrograph of a general view of sample G4. White square marks the area enlarged in b. b) SEM micrograph of the area marked in a, corresponding to the inner part of the tow. The BDD coating is marked by white arrows. c) Diamond coating area (A_D) in all coated samples. d) SEM micrograph of BDD coated CF and an enlargement of the diamond surface (Sample G4) e) SEM micrograph of sample G6. The CF surface coated with carbon nanowalls is shown by white arrows and an enlargement of the surface.

Table 3
Dimensions of the deposited diamond. A_D is the growth diamond area and t the thickness of the diamond layer of all samples.

#	G1	G2	G3	G4	G5	G6
$A_D(\mu m^2)$	712	2966	22,510	16,322	10,025	433
t(nm)	79	85	69	104	79	90

cm^{-1} attributed to sp^2 carbon bonds, (labelled D-band and G-band in Fig. 3, respectively) [46]. In the spectra of BDD samples, a band located at 1200 cm^{-1} (labelled as Boron band in Fig. 3) attributed to the boron dopant is shown. The diamond peak (sp^3 carbon bonds) appears in the range 1300–1332 cm^{-1} (labelled as sp^3 in Fig. 3), shifted to a lower wavelength by the action of boron [47]. A significant broad band is observed in the range 1460–1560 cm^{-1}, which may be associated with non-diamond related carbon phases (labelled sp^2 G-band in Fig. 3) [48]. D-band also is slightly showed in G1-G7 samples.

Boron doping levels have been evaluated using the method proposed by V. Mortet et al. [35,49–51] (Table 4). Boron concentration values in Table 4 are the average of five Raman spectroscopy doping level measurements carried out at different location of coated CF (The relevant data supporting these results can be found in the supplementary material Figs. S1-S6 and Table S1). The boron doping level resulted in the range of 2- $5\bullet10^{21}$ cm^{-3} for samples G2-7. G1 did not exhibit any doping since no boron precursors were used during its growth. In this way, this sample only presents a residual doping outside the detection range of the method used. The difference observed in the boron content between the different samples can be attributed to the variation in temperature induces by changes in the gas pressure.

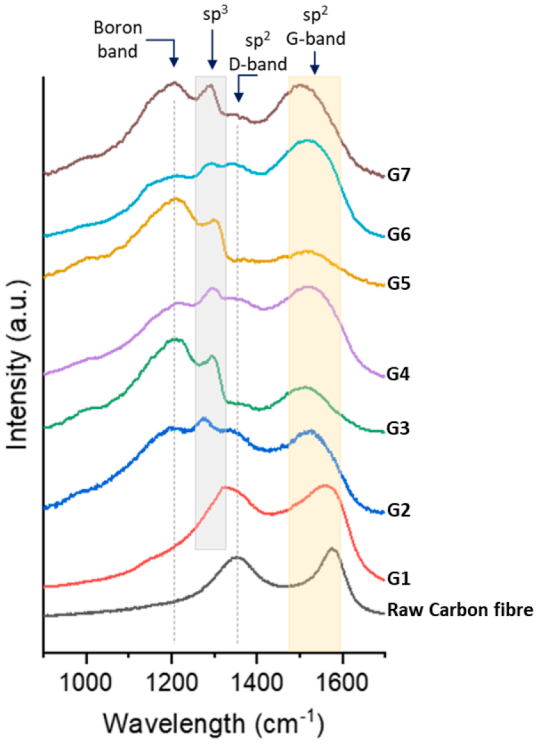

Fig. 3. Room-temperature corrected Raman spectra of grown BDD-CF samples and uncoated carbon fibre.

3.1. Kelvin method

For comparison purposes, the Kelvin method measurements were carried out on the coated samples as well as on an uncoated CF. Fig. 4a shows the resistance of the uncoated CF measured at various lengths (SEM micrograph in the supplementary material Fig. S7). As expected, CF exhibits ohmic (linear) behaviour with an electrical conductivity value of 58.8 (±0.2) $\Omega^{-1}\bullet mm^{-1}$ [52]. This trend, shown as a red line in the figure, indicates a relatively good uniformity of electrical characteristics along the length of the CF. The behaviour with respect to the measurement length gives confidence in the method used to derive the electrical conductivity. The linear fit shows a zero length resistance of

Table 4
Boron concentration in doped diamond coatings on carbon fibres and pressure during the growth.

Nomenclature	G1	G2	G3	G4	G5	G6	G7
Boron concentration(cm^{-3})	$<5.10^{19}$	3.10^{21}	4.10^{21}	3.10^{21}	3.10^{21}	2.10^{21}	4.10^{21}
Pressure(Torr)	35	40	35	40	45	45	35

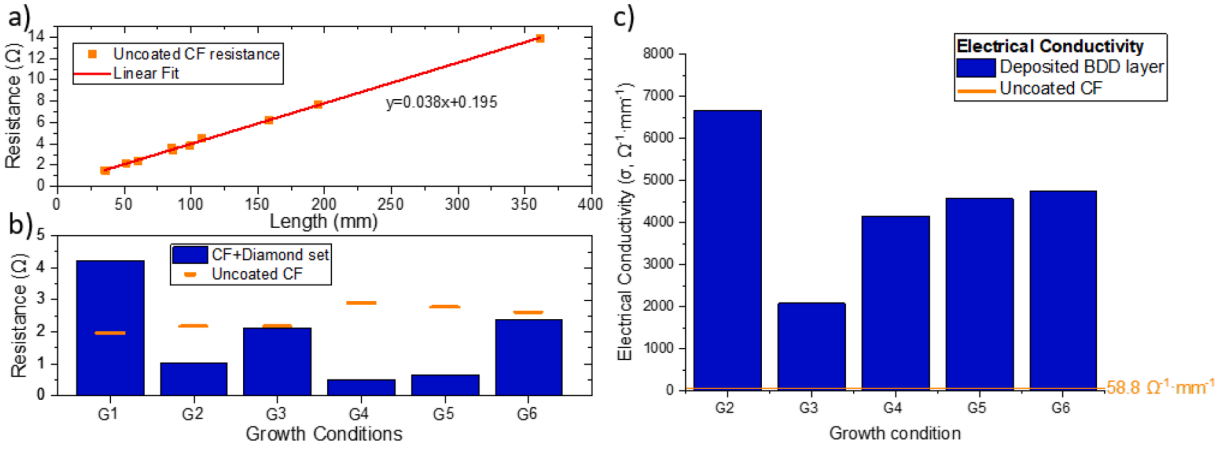

Fig. 4. a) Resistance-length curve behaviour carried out on an uncoated CF tow using the Kelvin method. b) Resistance of BDD-CF set tow measured by kelvin method, each column corresponds to a different growth condition. Oranges lines correspond with uncoated CF resistances with the same samples length c) Electrical conductivity of the BDD coating for each growth condition used.

0.195 Ω attributed to the contact resistance measurement.

The results of the Kelvin measurements of the BDD-CF are shown in Fig. 4b.These results are the average of several measurements made on different CF grown in the same batch. The bar graph shows the ohmic resistances of a CF coated tow of each sample. The orange lines set the CF resistance for the same length as BDD-CF tows. Sample G1, grown without boron precursor gas, shows the highest resistance value (4.2 Ω). This resistance is higher than the uncoated CF for the same length of fibre (2 Ω) since lightly-boron-doped diamond is a poorer electrical conductor than CF.

Samples G3 and G6 have resistance similar to uncoated CF (2.1 and 2.4 Ω, respectively). The resistivities observed in G3 and G6 are due to inhomogeneity on the BDD layer, and the high percentage of CF coated only with carbon nanowalls observed by SEM (Fig. 2d, more detailed in the supplementary material Figure S8 and S9). On the other hand, samples G2, G4 and G5 have homogenous BDD coating from the centre to the surface of the tows, as shown in Fig. 2a-b. The high percentage of coated CF leads to low electrical resistances compare to uncoated CF (orange lines). In fact, the electrical resistance of the tow was reduced from half (sample G2) to 5 times (sample G4), which is attributed to the BDD coating.

From these results, the electrical conductivity of the BDD layer can be estimated using the following equation:

$$\sigma_D = \frac{L \times \left(\frac{1}{R_T} - \frac{1}{R_{CF}}\right)}{A_D} \quad (1)$$

where σ_D is the electrical conductivity of the BDD layer, L is the length of the BDD coating, R_T is the measured electrical resistance of the set BDD-CF, R_{CF} is the CF electrical resistance and A_D is the estimated BDD coating area by SEM.

The electrical conductivity of the BDD coatings is plotted in Fig. 4c. Due to its non-conducting nature, the G1 sample is not included in this study. All the BDD layers of samples G2 to G6 show an electrical conductivity in the order of 10^3 $\Omega^{-1}\bullet mm^{-1}$, that is two orders of magnitude higher than that of the uncoated CF. The difference in the electrical conductivities between the samples is attributed to the different doping level and the lack of homogeneity of the BDD layer.

The good electrical conductivities (σ_D) shown in Fig. 4c ($\backsim 10^3$ $\Omega^{-1}\bullet mm^{-1}$) are due to the high level of boron doping of the samples obtained by Raman spectroscopy (Fig. 3). Boron concentrations (Table 4) were used together with the work of W. Gajewski et al. [53], to estimate the BBD electrical conductivity. As a result, BDD electrical conductivity values in the range of 10^2-10^3 $\Omega^{-1}\bullet mm^{-1}$ are obtained. These electrical conductivity values are in good agreement with those obtained by the Kelvin method (Fig. 4c).

3.2. Conductive AFM local measurements

Fig. 5a shows the electrical current map obtained on an uncoated CF by C-AFM. The surface electrical response reveals the characteristic longitudinal grooves of the CF bare surface, used to increase the fibre roughness, and favour the polymer-CF adhesion [8]. Here, the roughness (R_a) obtained by AFM was 12 nm in scanned area of 4 μm^2. The surface electrical behaviour of the uncoated fibre is homogeneous with values on the microamp scale.

Fig. 5b corresponds to the C-AFM map of sample G7. It shows a higher current response than that observed for the uncoated CF (Fig. 5a). The BDD-CF surface a wide distribution range of current values due to the granular structure of the polycrystalline BDD. As observed in the SEM micrographs (Fig. 2c), the CF is covered by nanocrystalline BDD grains that fill the grooves of the original CF. This coating reduces surface roughness resulting in an R_a of 9 nm in an area of 4 μm^2.

Fig. 5c shows the current distribution AFM map of both samples. Uncoated CF exhibits a narrow current distribution (full width at half maximum, FWHM of 0.52 μA) that is related to a more heterogeneous current density. This trend has been fitted to a single Gaussian function with a peak centred at 0.36 μA. On the other hand, the BDD-CF shows a broader current distribution highlighting the granular nature of the surface and its borders. This trend has also been fitted to a single Gaussian function with a peak centered at 2.08 μA and a FWHM of 3.38 μA. This comparative graph highlights the higher surface conductivity of the BDD coated CF, which increases by an order of magnitude.

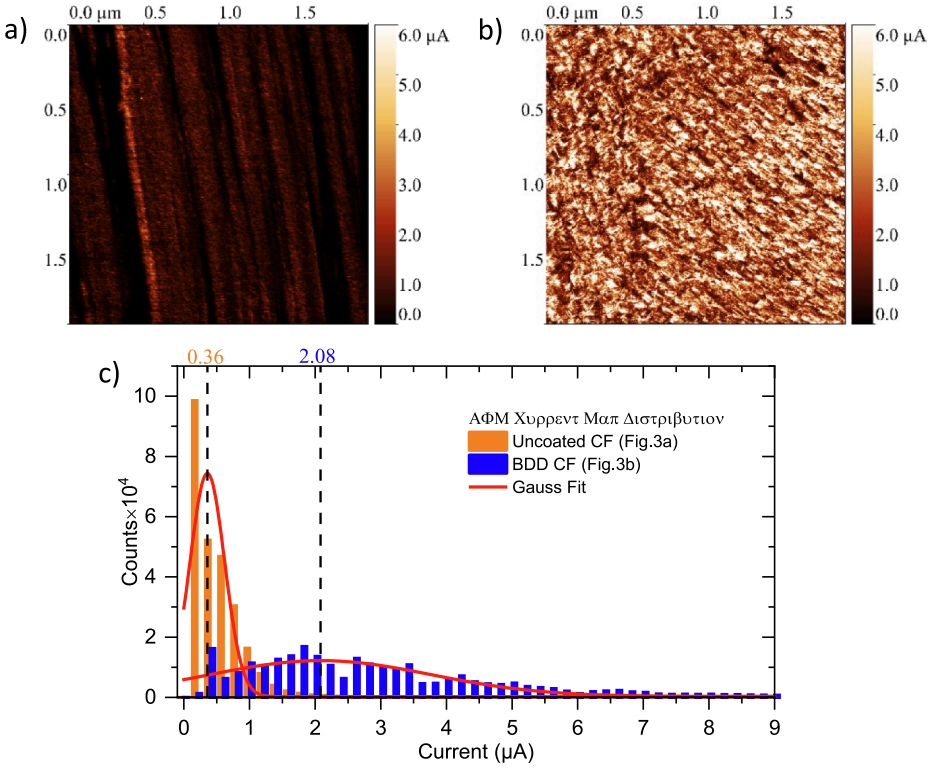

Fig. 5. a) C-AFM maps on an uncoated CF, b) C-AFM maps on BDD-CF, c) Surface current map histograms of both, uncoated CF (orange) and BDD-CF (blue), based on results from 4a and b. Both experiments were carried out at the same conditions (sample bias of + 500 mV, diamond coated tips CDT-NCHR (k = 80 N/m, f = 400 kHz), and both successively performed in 2 h). (For interpretation of the references to colour in this figure legend, the reader is referred to the web version of this article.)

3.3. sMIM/AFM

In order to have a smooth surface for scanning, the G7 sample was embedded in an epoxy resin and polished in cross-section as described in the methodology section. Topography (contact mode) and sMIM resistive signal (sMIM-R) maps were obtained simultaneously in a cross-section view of the vertical coated filaments within a 30 × 30 µm^2 scan size area.

Fig. 6a shows the sMIM-R map of BDD-CF on resin recorded in the forward scan direction (left to right scan), at a microwave frequency around 3 GHz. The surface electrical response of the sample is plotted in a red (0 V) to green (6.1 V) colour scale. Forward and backward scans show identical results.

Based on the different colours observed in Fig. 6a, three different electrical behaviour areas can be identified. Each of these areas corresponds to a sample compound: (i) resin used to embed the CF in dark red, (ii) CF core in orange, and (iii) BDD coating in yellow. The closer to yellow, the more electrically conductive the material is. Unfortunately, the colour representation cannot be quantified, but it allows comparison of the variation in relative electrical conductivities between these materials. The BDD coating exhibits higher conductivity than the CF core and both show higher conductivity than the resin, which is known to be an insulating material.

All the filaments were grown in the reactor in the same process and some of the fibres were partially covered by the others. The directional effect of the BDD deposition results in a thicker coverage on the surface of the side that was more exposed to the plasma during the deposition process. In this way, the thickness of the BDD layer varies in the same fibers. Fig. 6a shows the effect of this directional growth.

The sMIM-R voltage map distribution is shown in Fig. 6b. The

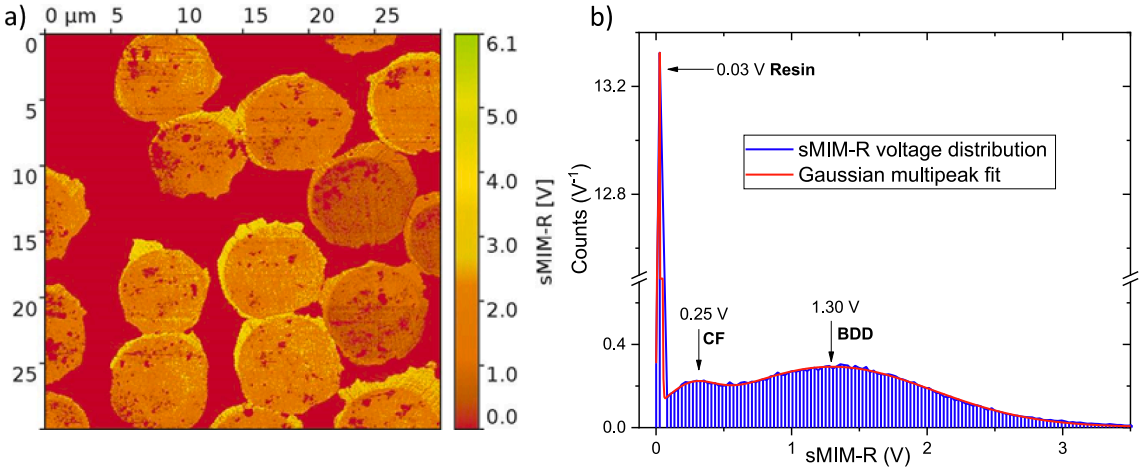

Fig. 6. sMIM cross-sectional measurement on BDD-CF upright standing position. a) sMIM-Resistive signal map scan in forward direction. b) sMIM-Resistive signal distribution of the same region.

obtained histogram clearly shows three voltage peaks that have been fitted with Gaussian functions. The first peak corresponds to a low voltage value of 0.03 V, that has been attributed to the resin. The second peak is centred at 0.25 V and corresponds to the CF core. Finally, the third peak, centred at 1.30 V, is attributed to the BDD coating. The electrical response obtained from the BDD coating is one order of magnitude higher than that obtained from the CF core. This result agrees with the results of C-AFM and the Raman estimations.

4. Conclusions

The electrical effects of the BDD coating on the carbon fibres have been studied using the Kelvin method (2-wire), C-AFM and sMIM/AFM modes. The BDD coating on CF improves the electrical conductivity at micro and macro scale.

The Kelvin macro measurement reflects a great improvement in the electrical conductivity of the BDD-CF compared to the uncoated CF. The BDD grown on carbon fibres decreases the electrical resistance of the BDD-CF set by at least half compared to the uncoated CF. The electrical conductivity of BDD coating was estimated to be greater than 10^3 $\Omega^{-1}\bullet mm^{-1}$ by the Kelvin method and Raman spectroscopy.

On the other hand, the measured local surface electrical response of a single BDD-CF filament shows an improvement over uncoated CF. Micro measurement via C-AFM reveals an order of magnitude increase in surface conductivity in the coated CFs.

sMIM allowed the study of the cross-sectional sample avoiding the influence of the resin matrix. The sMIM-R results support an order of magnitude difference in surface electrical response between fibre and BDD coating obtained by C-AFM. sMIM-Resistive signal measurements reveal the presence of ring-shaped deposited structures around the CFs and identify this ring as the BDD coating. The three materials have been identified based on their electrical behaviour: resin, CF and BDD.

Once demonstrated the improvement in the longitudinal electrical conductivity of individual BDD-CF. The electrical behaviour of CFRP is also expected to improve in the transverse direction due to the percolation effect of the diamond grains. In a CFRP material, the BDD-CFs will touch each other through the BDD coating. In this way, a transverse conductive path will be created. Therefore, the electrical conductivity will increase, and the electrical anisotropy of the material will decrease. This will allow a wider range of applications in the biomedical, aeronautical, and structural fields.

CRediT authorship contribution statement

J. Millán-Barba: Conceptualization, Methodology, Formal analysis, Investigation, Data curation, Writing – original draft, Writing – review & editing, Visualization. **H. Bakkali:** Investigation, Formal analysis. **F. Lloret:** Validation, Resources, Supervision, Funding acquisition. **M. Gutiérrez:** Validation, Conceptualization, Supervision, Funding acquisition. **R. Guzmán de Villoria:** Supervision, Funding acquisition. **M. Domínguez:** Validation, Supervision. **K. Haenen:** Funding acquisition, Resources. **D. Araujo:** Validation, Conceptualization, Resources, Supervision, Funding acquisition.

Declaration of Competing Interest

The authors declare the following financial interests/personal relationships which may be considered as potential competing interests: Josue Millan Barba reports financial support was provided by Foundation for the Research, Development and Application of Composite Materials.

Data availability

Data will be made available on request.

Acknowledgement

The authors thank the Ministerio de Economía y Empresa (MINECO) Spanish Government for funding under grant N° PID2019-110219RB-100 and N° PID2020-117201RB-C21, as well as the co-financing by the 2014-2020 ERDF Operational Programme, the funding grants N° PY20_00946 and N° FEDER-UCA18-107851 and by the Department of Economy, Knowledge, Business and University of the Regional Government of Andalusia. Project reference: FEDER-UCA18-107851. M. Dominguez acknowledges the support by the Spanish Ministerio de Ciencia, Innovación y Universidades under project EQC2018-004704-P. They are also grateful to FIDAMC and the University of Salamanca. K.H. thanks the Methusalem "Nano'' network.

Appendix A. Supplementary data

Supplementary data to this article can be found online at https://doi.org/10.1016/j.apsusc.2023.156382.

References

[1] M. Mrazova, Advanced composite materials of the future in aerospace industry, INCAS Bull. 5 (2013) 139–150, https://doi.org/10.13111/2066-8201.2013.5.3.14.
[2] N.M. Aly, A review on utilization of textile composites in transportation towards sustainability, IOP Conf. Ser.: Mater. Sci. Eng. 254 (2017), https://doi.org/10.1088/1757-899X/254/4/042002.
[3] D. Tang, The Application of Carbon Fiber Materials in Sports Equipment, Appl. Mech. Mater. 443 (2013) 613–616, https://doi.org/10.4028/www.scientific.net/AMM.443.613.
[4] N. Forintos, T. Czigany, Multifunctional application of carbon fiber reinforced polymer composites: Electrical properties of the reinforcing carbon fibers – A short review, Compos. Part B Eng. 162 (2019) 331–343, https://doi.org/10.1016/j.compositesb.2018.10.098.
[5] J. Zhang, T. Lin, X. Wang, 4 - Carbon and polymer nanofiber reinforcements in polymer matrix composites: processing and applications, in: Funct. Nanofibers Their Appl , Woodhead Publishing Limited, 2012, pp. 55–70. https://doi.org/10.1533/9780857095640.1.55.
[6] M.S. Ha, O.Y. Kwon, H.S. Choi, A Study of Electrical Conductivity Improvement of Carbon-Fiber Reinforced Plastics by Conductive Nano-Particles Coating, Conf. Korean Soc. Compos. Mater. (2008) 255–259.
[7] S. Tiwari, J. Bijwe, Surface Treatment of Carbon Fibers - A Review, Procedia Technol. 14 (2014) 505–512, https://doi.org/10.1016/j.protcy.2014.08.064.
[8] M. Sharma, S. Gao, E. Mäder, H. Sharma, L.Y. Wei, J. Bijwe, Carbon fiber surfaces and composite interphases, Compos. Sci. Technol. 102 (2014) 35–50, https://doi.org/10.1016/j.compscitech.2014.07.005.
[9] E. Kandare, A.A. Khatibi, S. Yoo, R. Wang, J. Ma, P. Olivier, et al., Improving the through-thickness thermal and electrical conductivity of carbon fibre/epoxy laminates by exploiting synergy between graphene and silver nano-inclusions, Compos. Part A Appl. Sci. Manuf. 69 (2015) 72–82, https://doi.org/10.1016/j.compositesa.2014.10.024.
[10] S. Zhang, L. Gao, J. Han, Z. Li, G. Zu, X. Ran, et al., Through-thickness thermal conductivity enhancement and tensile response of carbon fiber-reinforced polymer composites, Compos. Part B Eng. 165 (2018) 183–192, https://doi.org/10.1016/j.compositesb.2018.11.114.
[11] X. Zheng, S. Kim, C. Woo Park, Enhancement of thermal conductivity of carbon fiber-reinforced polymer composite with copper and boron nitride particles, Compos. Part A. Appl. Sci. Manuf. 121 (2019) 449–456, https://doi.org/10.1016/j.compositesa.2019.03.030.
[12] N. Yamamoto, R.G. De Villoria, B.L. Wardle, Electrical and thermal property enhancement of fiber-reinforced polymer laminate composites through controlled implementation of multi-walled carbon nanotubes, Compos. Sci. Technol. 72 (2012) 2009–2015, https://doi.org/10.1016/j.compscitech.2012.09.006.
[13] N. De Greef, L. Zhang, A. Magrez, L. Forró, J. Locquet, I. Verpoest, et al., Direct growth of carbon nanotubes on carbon fibers : Effect of the CVD parameters on the degradation of mechanical properties of carbon fibers, Diam. Relat. Mater. 51 (2015) 39–48, https://doi.org/10.1016/j.diamond.2014.11.002.
[14] S. Koizumi, C. Nebel, M. Nesladek (Eds.), Physics and Applications of CVD Diamond, 2008.
[15] B.-L. Anderson, R. Anderson (Eds.), Fundamentals of Semiconductor Devices, Second Edi, McGRAW-HILL Education international edition, New York, 2018.
[16] D. Araujo, M. Suzuki, F. Lloret, G. Alba, P. Villar, Diamond for Electronics : Materials, Processing and Devices, Materials (Basel). 14 (2021) 7081, https://doi.org/10.3390/ma14227081.
[17] L.S. Pan, D.R. Kania, eds., Diamond: Electronic properties and aplications, Springer Science + Business Media, LLC, 2018. doi:10.1007/978-1-4615-2257-7.
[18] J.J. Gracio, Q.H. Fan, J.C. Madaleno, Diamond growth by chemical vapour deposition, J. Phys. D. Appl. Phys. 43 (2010), https://doi.org/10.1088/0022-3727/43/37/374017.

[19] J.H.T. Luong, K.B. Male, J.D. Glennon, Boron-doped diamond electrode: Synthesis, characterization, functionalization and analytical applications, Analyst. 134 (2009) 1965–1979, https://doi.org/10.1039/b910206j.
[20] F.S. Manciu, Y. Oh, A. Barath, A.E. Rusheen, A.Z. Kouzani, D. Hodges, et al., Analysis of Carbon-Based Microelectrodes for Neurochemical Sensing, Materials (Basel). 12 (2019), https://doi.org/10.3390/ma12193186.
[21] C.-M. Niu, G. Tsagaropoulos, J. Baglio, K. Dwight, A. Wold, Nucleation and Growth of Diamond on Si, Cu, and Au Substrates, J. Solid State Chem. 91 (1991) 47–56, https://doi.org/10.1016/0022-4596(91)90056-N.
[22] W. Kulisch, C. Popov, V. Vorlicek, P.N. Gibson, G. Favaro, Nanocrystalline diamond growth on different substrates, Thin Solid Films. 515 (2006) 1005–1010, https://doi.org/10.1016/j.tsf.2006.07.163.
[23] J. Echigoya, H. Enoki, S. Kaminishi, Growth of diamond films on SiC, WC and cubic BN substrates, J. Mater. Sci. 32 (1997) 4693–4699, https://doi.org/10.1023/A:1018662410280.
[24] X.C. He, H.S. Shen, Z.M. Zhang, X.J. Hu, Y.Z. Wan, T. Shen, Growth of CVD heteroepitaxial diamond on silicon (001) and its electronic properties, Diam. Relat. Mater. 9 (2000) 1626–1631, https://doi.org/10.1016/S0925-9635(00)00317-4.
[25] H.O. Pierson. Handbook of chemical vapor deposition. Principles, Technology and Applications, Second edi, Noyes Publications, New York, 1999.
[26] J. Barjon, N. Habka, C. Mer, F. Jomard, J. Chevallier, P. Bergonzo, Resistivity of boron doped diamond, Phys. Status Solidi - Rapid Res. Lett. 3 (2009) 202–204, https://doi.org/10.1002/pssr.200903097.
[27] V. Petrák, Z. Vlčková Živcová, H. Krýsová, O. Frank, A. Zukal, L. Klimša, et al., Fabrication of porous boron-doped diamond on SiO2 fiber templates, Carbon N. Y. 114 (2017) 457–464, https://doi.org/10.1016/j.carbon.2016.12.012.
[28] Z. Vlčková Živcová, V. Mortet, A. Taylor, A. Zukal, O. Frank, L. Kavan, Electrochemical characterization of porous boron-doped diamond prepared using SiO2 fiber template, Diam. Relat. Mater. 87 (2018) 61–69, https://doi.org/10.1016/j.diamond.2018.05.007.
[29] F. Omnès, P. Muret, P.-N. Volpe, M. Wade, J. Pernot, F. Jomard, Study of boron doping in MPCVD grown homoepitaxial diamond layers based on cathodoluminescence spectroscopy, secondary ion mass spectroscopy and capacitance-voltage measurements, Diam. Relat. Mater. 20 (2011) 912–916, https://doi.org/10.1016/j.diamond.2011.05.010.
[30] J. Barjon, P. Desfonds, M.-A. Pinault, T. Kociniewski, F. Jomard, J. Chevallier, Determination of the phosphorus content in diamond using cathodoluminescence spectroscopy, J. Appl. Phys. 101 (2007), https://doi.org/10.1063/1.2735408.
[31] C. Fernández-Lorenzo, D. Araújo, M. González-Mañas, J. Martín, J. Navas, R. Alcántara, et al., Multi-technique analysis of high quality HPHT diamond crystal, J. Cryst. Growth. 353 (2012) 115–119, https://doi.org/10.1016/j.jcrysgro.2012.05.007.
[32] D. Araújo, M.A. Paz Alegre, A.J. García, M. Pilar Villar, E. Bustarret, P. Achatz, et al., Cross sectional evaluation of boron doping and defect distribution in homoepitaxial diamond layers, Phys. Status Solidi Curr. Top. Solid State Phys. 8 (2011) 1366–1370, https://doi.org/10.1002/pssc.201083991.
[33] N. Ohtake, M. Hiratsuka, K. Kanda, H. Akasaka, M. Tsujioka, K. Hirakuri, et al., Properties and Classification of Diamond-Like Carbon Films, Materials (Basel). 14 (2021), https://doi.org/10.3390/ma14020315.
[34] M. Bernard, A. Deneuville, P. Muret, Non-destructive determination of the boron concentration of heavily doped metallic diamond thin films from Raman spectroscopy, Diam. Relat. Mater. 13 (2004) 282–286, https://doi.org/10.1016/j.diamond.2003.10.051.
[35] V. Mortet, Z.V. Živcová, A. Taylor, M. Davydová, O. Frank, P. Hubík, et al., Determination of atomic boron concentration in heavily boron-doped diamond by Raman spectroscopy, Diam. Relat. Mater. 93 (2019) 54–58, https://doi.org/10.1016/j.diamond.2019.01.028.
[36] B.A. Newcomb, Processing, structure, and properties of carbon fibers, Compos. Part A Appl. Sci. Manuf. 91 (2016) 262–282, https://doi.org/10.1016/j.compositesa.2016.10.018.
[37] X. Qian, J. Zhi, L. Chen, J. Zhong, X. Wang, Y. Zhang, et al., Evolution of microstructure and electrical property in the conversion of high strength carbon fiber to high modulus and ultrahigh modulus carbon fiber, Compos. Part A Appl. Sci. Manuf. 112 (2018) 111–118, https://doi.org/10.1016/j.compositesa.2018.05.030.
[38] M.M. Ghorbani, R. Taherian, 12 - Methods of Measuring Electrical Properties of Material, in: R. Taherian, A. Kausar (Eds.), Electr. Conduct. Polym, Compos., William Andrew Publishing, 2019, pp. 365–394, https://doi.org/10.1016/B978-0-12-812541-0.00012-4.
[39] S.I. Shah, M.M. Waite, Diamond deposition on carbon fibers, J. Vac. Sci. Technol. A Vacuum, Surfaces, Film. 13 (1995) 1624–1627, https://doi.org/10.1116/1.579741.
[40] M. Marton, M. Vojs, M. Kotlár, P. Michniak, L. Vančo, M. Veselý, et al., Deposition of boron doped diamond and carbon nanomaterials on graphite foam electrodes, Appl. Surf. Sci. 312 (2014) 139–144, https://doi.org/10.1016/j.apsusc.2014.05.199.
[41] S.S. Nicley, S. Drijkoningen, P. Pobedinskas, J. Raymakers, W. Maes, K. Haenen, Growth of Boron-Doped Diamond Films on Gold-Coated Substrates with and without Gold Nanoparticle Formation, Cryst. Growth Des. 19 (2019) 3567–3575, https://doi.org/10.1021/acs.cgd.9b00488.
[42] J. Millán-Barba, M. Gutiérrez, F. Lloret, R. Guzmán de Villoria, R. Alcántara, K. Haenen, et al., Study of early stages in the growth of boron-doped diamond on carbon fibers, Phys. Status Solidi Appl. Mater. Sci. 218 (2020), https://doi.org/10.1002/pssa.202000284.
[43] Y. Wang, T.H. Hahn, AFM characterization of the interfacial properties of carbon fiber reinforced polymer composites subjected to hygrothermal treatments, Compos. Sci. Technol. 67 (2007) 92–101, https://doi.org/10.1016/j.compscitech.2006.03.030.
[44] H. Thierschmann, H. Cetinay, M. Finkel, A.J. Katan, M.P. Westig, P. Van Mieghem, et al., Local Electrodynamics of a Disordered Conductor Model System Measured with a Microwave Impedance Microscope, Phys. Rev. Appl. 13 (2020), 014039, https://doi.org/10.1103/PhysRevApplied.13.014039.
[45] K.A. Rubin, Y. Yang, O. Amster, D.A. Scrymgeour, S. Misra, Scanning Microwave Impedance Microscopy (sMIM) in Electronic and Quantum Materials, Electr. At. Force Microsc. Nanoelectron., Springer International Publishing (2019) 385–408, https://doi.org/10.1007/978-3-030-15612-1.
[46] A. Carlo Ferrari, J. Robertson, Raman spectroscopy of amorphous, nanostructured, diamond-like carbon, and nanodiamond, Philos. Trans. R. Soc. A Math. Phys. Eng. Sci. 362 (2004) 2477–2512, https://doi.org/10.1098/rsta.2004.1452.
[47] H.A. Bland, E.L.H. Thomas, G.M. Klemencic, S. Mandal, D.J. Morgan, A. Papageorgiou, et al., Superconducting Diamond on Silicon Nitride for Device Applications, Sci. Rep. 9 (2019), https://doi.org/10.1038/s41598-019-39707-z.
[48] J.A.N. Gonçalves, G.M. Sandonato, K. Iha, Characterization of boron doped CVD diamond films by Raman spectroscopy and X-ray diffractometry, Diam. Relat. Mater. 11 (2002) 1578–1583., https://doi.org/10.1016/S0925-9635(02)00103-6.
[49] V. Mortet, Z. Vlčková Živcová, A. Taylor, O. Frank, P. Hubík, D. Trémouilles, et al., Insight into boron-doped Diamond Raman Spectra Characteristic features, Carbon N. Y. 115 (2017) 279–284, https://doi.org/10.1016/j.carbon.2017.01.022.
[50] V. Mortet, A. Taylor, Z. Vlčková Živcová, D. Machon, O. Frank, P. Hubík, et al., Analysis of heavily boron-doped diamond Raman spectrum, Diam. Relat. Mater. 88 (2018) 163–166, https://doi.org/10.1016/j.diamond.2018.07.013.
[51] V. Mortet, I. Gregora, A. Taylor, N. Lambert, P. Ashcheulov, Z. Gedeonova, et al., New perspectives for heavily boron-doped diamond Raman spectrum analysis, Carbon N. Y. 168 (2020) 319–327, https://doi.org/10.1016/j.carbon.2020.06.075.
[52] V. Safarova, J. Gregr, Electrical Conductivity Measurement of Fibers and Yarns, 7th Int. Conf. - TEXSCI. (2010) 2–9.
[53] W. Gajewski, P. Achatz, O.A. Williams, K. Haenen, E. Bustarret, M. Stutzmann, et al., Electronic and optical properties of boron-doped nanocrystalline diamond films, Phys. Rev. B - Condens. Matter Mater. Phys. 79 (2009) 1–14, https://doi.org/10.1103/PhysRevB.79.045206.